

# Hyperthermia Effect of Nanoclusters Governed by Interparticle Crystalline Structures

Miseon Jeong, Sanghoon Lee, Dae Young Song, Sunghwi Kang, Tae-Hyun Shin, and Jin-sil Choi\*



Cite This: *ACS Omega* 2021, 6, 31161–31167



Read Online

ACCESS |



Metrics & More

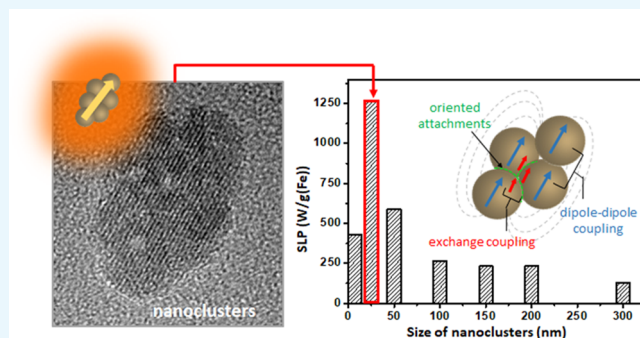


Article Recommendations



Supporting Information

**ABSTRACT:** Magnetic nanoparticles have an important role as heat generators in magnetic fluid hyperthermia, a type of next-generation cancer treatment. Despite various trials to improve the heat generation capability of magnetic nanoparticles, iron oxide nanoparticles are the only approved heat generators for clinical applications, which require a large injection dose due to their low hyperthermia efficiency. In this study, iron oxide nanoclusters (NCs) with a highly enhanced hyperthermia effect and adjustable size were synthesized through a facile and simple solvothermal method. Among the samples, the NCs with a size of 25 nm showed the highest hyperthermia efficiency. Differently sized NCs exhibit inconsistent interparticle crystalline alignments, which affect their magnetic properties (e.g., coercivity and saturation magnetization). As a result, the optimal NCs exhibited a significantly enhanced heat generation efficiency compared with that of isolated iron oxide nanoparticles (ca. 7 nm), and their hyperthermia effect on skin cancer cells was confirmed.

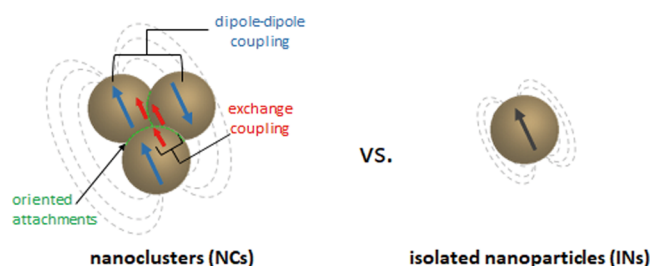


## 1. INTRODUCTION

Magnetic fluid hyperthermia (MFH) using magnetic nanoparticles as heat mediators has attracted interest for cancer therapy because of its noninvasiveness, localized therapeutic capability, and lack of therapeutic limits depending on the type of cancer.<sup>1–5</sup> The heat generation capability of iron oxide, the most frequently employed heat generator platform, can be controlled by doping of other metals or varying the size or shape (Table S1). For example, the introduction of dopants such as Co, Mn, or Zn can increase the magnetic anisotropy,<sup>3,6–9</sup> leading to enhanced heat generation. Additionally, the heat dissipation of composite ferrites with a core-shell structure is much greater than that of pure iron oxide due to exchange coupling between soft ferrites (e.g.,  $\text{Zn}_{0.4}\text{Fe}_{2.6}\text{O}_4$ ) and hard ferrites (e.g.,  $\text{CoFe}_2\text{O}_4$ ).<sup>10,11</sup> Despite these advances toward establishing superior hyperthermia properties, pure iron oxide is the only inorganic material that has been approved by the Food and Drug Administration (FDA), while ferrite materials containing doped metals require verification of their biocompatibility for clinical applications. Therefore, the development of iron oxide nanoparticles with high heat generation efficiencies is warranted for clinical use, especially for cancer treatment.

Aside from the aid of additional dopants, interparticle interactions are another<sup>12–15</sup> promising tool to regulate the hyperthermia effect of iron oxide nanoparticles (Scheme 1). Interparticle interactions are generally dipole–dipole coupling or exchange coupling, where the former is a long-range interaction between separate dipoles<sup>14,16</sup> and the latter occurs

## Scheme 1. Schematic Comparing the Magnetic Properties of an Isolated Nanoparticle and Nanocluster (NC)



between tightly bound magnetic spins.<sup>5</sup> Nanoclusters (NCs) are composed of multiple magnetic cores assembled to form a well-defined structure that exhibits a collective magnetic behavior due to interparticle interactions between cores, which affects their hyperthermia efficiency.<sup>2,17,18</sup> Various types of iron oxide NCs can be obtained through chemical synthesis, post-conjugation, template-mediated assembly, or encapsulation.<sup>2,17</sup> However, the NCs obtained through post-conjugation, template assembly, or encapsulation of individual

Received: August 25, 2021

Accepted: October 29, 2021

Published: November 10, 2021



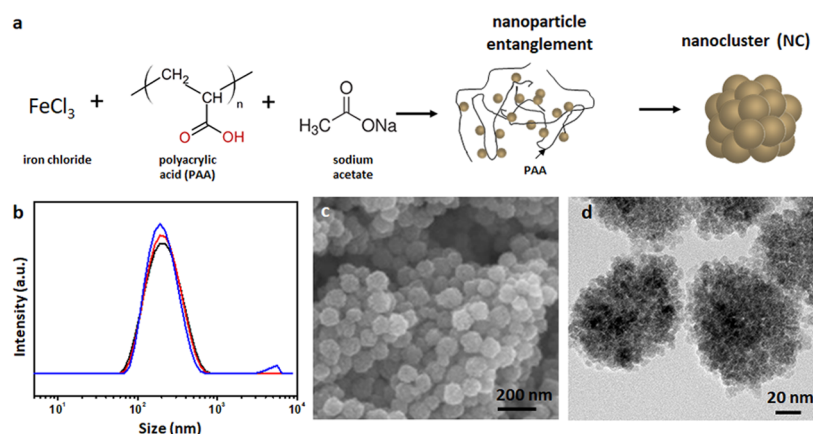


**Figure 1.** (a) Schematic of NC synthesis, (b) hydrodynamic size, (c) SEM image, and (d) TEM image of NC\_150.

nanoparticles are disadvantageous for mass production.<sup>12,19</sup> Therefore, it is important to develop iron oxide NC systems with effective hyperthermia properties through facile and one-pot synthetic methods. In addition, most studies have focused on comparing the hyperthermia effect of NCs and isolated nanoparticles, whereas the hyperthermia effect of NCs themselves is still debatable.<sup>12,13,20–22</sup> In this study, we prepared pure iron oxide NCs with an enhanced hyperthermia effect by a simple solvothermal method<sup>15,17,23–32</sup> in which the NC size can be controlled by changing the reaction parameters. We demonstrate that interparticle crystalline structure-dependent magnetic properties strongly influence the hyperthermia effect of the iron oxide NCs. With our comprehensive investigation, we demonstrate an optimal and practical iron oxide-based heat generator for MFH.

## 2. RESULTS AND DISCUSSION

Iron oxide NCs were synthesized *via* a solvothermal method using poly(acrylic acid) (PAA) to stabilize the surface of iron oxide nanoparticles (Figure 1a). The purified particles displaying a dark brown color were stably dispersed in an aqueous solution, and their average hydrodynamic size was measured as  $\sim 190$  nm (Figure 1b). The rich carboxyl groups of PAA on the NCs resulted in a negative surface charge of  $-28$  eV (Figure S1), and the X-ray diffraction (XRD) pattern and X-ray photoelectron spectroscopy (XPS) indicated that the obtained NCs were magnetite ( $\text{Fe}_3\text{O}_4$ ) (Figures S2 and S3).<sup>33,34</sup> As determined by scanning electron microscopy (SEM) and transmission electron microscopy (TEM), the NCs were composed of compactly assembled iron oxide nanoparticles (*ca.* 7 nm) with an average cluster size of 150 nm for NC\_150 (Figure 1c,d). NC\_150 could be stably dispersed in an aqueous solution at pH 4–9 and salt concentrations up to 200 mM (Figure S5).

The size of the NCs can be controlled to 25, 50, 100, 150, 200, or 300 nm by changing the basicity of the reaction solution and the amount of PAA, as shown in Figure 2. Since the nanoparticles are clustered by entanglement on PAA to reduce their high surface energy, the size of the NCs could be modulated by controlling the coordination of the stabilizer. In the synthetic reaction, NaOAc as the base forms hydroxyl ions and generates iron hydroxides, which further condense to yield  $\text{Fe}_3\text{O}_4$ . When a strong base such as NaOH is also added, the reaction solvent (*i.e.*, ethylene glycol) can also be deprotonated, generating alkoxides that can also coordinate onto the

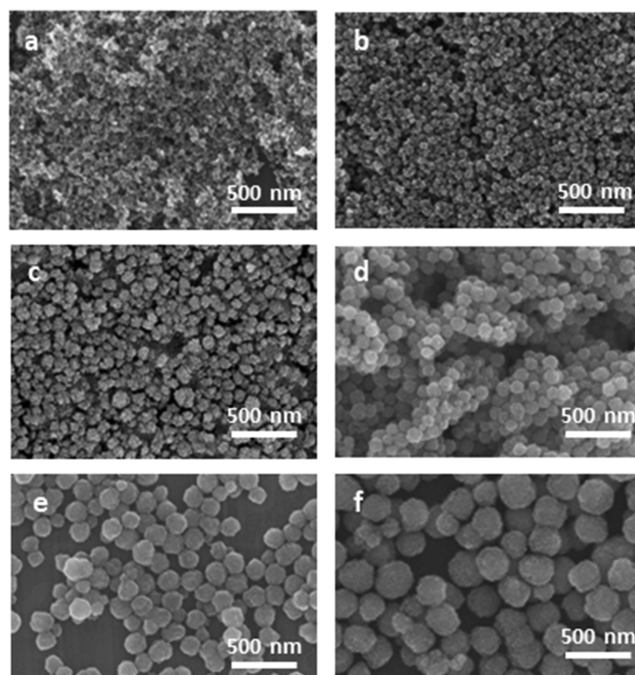


**Figure 2.** Size control of NCs. SEM images of NCs with average diameters of (a) 25, (b) 50, (c) 100, (d) 150, (e) 200, and (f) 300 nm. Each NC has a spherical shape and monodisperse size distribution.

nanoparticle surfaces.<sup>35</sup> Therefore, the use of a larger amount of NaOH results in smaller NCs. Accordingly, the size of the NCs decreased from 150 (NC\_150) to 100 (NC\_100), 50 (NC\_50), and 25 (NC\_25) nm by changing the ratio of NaOAc:NaOH from 1:0 to 1:0.1, 1:0.17, and 1:0.33, respectively (Figure 2a–d). To synthesize larger NCs, the amount of stabilizer (*e.g.*, PAA) is reduced. Since this renders the surface passivation insufficient, nanoparticle clustering is facilitated to minimize their surface energy, resulting in large NCs with sizes of 200 and 300 nm (NC\_200 and NC\_300, respectively) (Figure 2e,f). The hydrodynamic sizes of NC 25–300 were measured as 120.4, 62.2, 137.8, 146.1, 242.3, 267.2, and 296.2 nm (Figure S6).

The hyperthermia effect of the differently sized NCs was next explored. The electromagnetic energy of magnetic materials generated from magnetic spin fluctuation under an AMF transforms into another type of energy, heat. NC\_25 (1



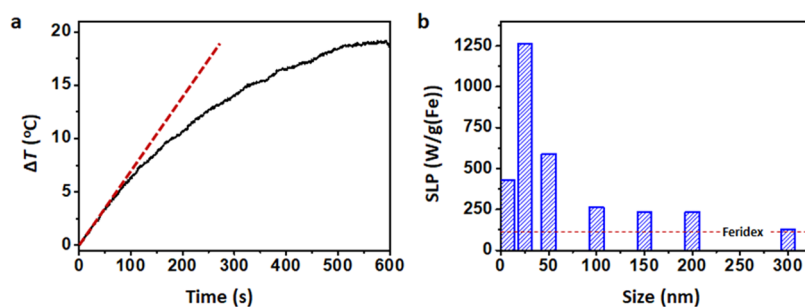


**Figure 3.** (a) Change in temperature *vs* time of NC\_25 under an AMF of 500 kHz and 37.5 kA·m<sup>-1</sup>. (b) SLP values of NCs calculated with the initial slope of the change in temperature *vs* time graph (control, red dotted line: Feridex).

mg·mL<sup>-1</sup>) can warm an aqueous solution under an AMF (500 kHz, 37.4 kA·m<sup>-1</sup>) by *ca.* 17 °C within 5 min (Figure 3a). The heat generation efficiency of the NCs was quantified according to specific loss power (SLP) values calculated by the initial slope method (Figure 3b). Isolated 7 nm iron oxide nanoparticles (IN\_7), which are similar in size to the nanoparticles comprising the NCs, were utilized as a control (Figure S7). Additionally, the SLP value of the commercially available iron oxide nanoparticle, Feridex (FDA approved iron oxide nanoparticles, Bayer HealthCare Pharmaceuticals Inc., Germany), was also measured. Among the NCs in this study, NC\_25 possessed a significantly enhanced SLP value of 1264 W·g<sup>-1</sup> (Fe), which is *ca.* 10 times higher than that of the Feridex. On the other hand, the SLP value of NC\_50 was 586 W·g<sup>-1</sup> (Fe), only slightly higher than that of IN-7, and the SLP values of NC\_100, NC\_150, NC\_200, and NC\_300 were even lower at 264, 231, 234, and 130 W·g<sup>-1</sup> (Fe), respectively. The SLP values of commercially available iron oxide (Feridex) under the same experimental conditions were measured as 127.9 and 240.5 W·g<sup>-1</sup>. Based on these observations, NC\_25 seems to be optimal as a hyperthermia agent.

To understand this phenomenon, the magnetic properties of the NCs were investigated.<sup>5</sup> The hysteresis graphs of the NCs were obtained under an external magnetic field from -5000 to 5000 Oe at room temperature (Figure 4). The magnetization

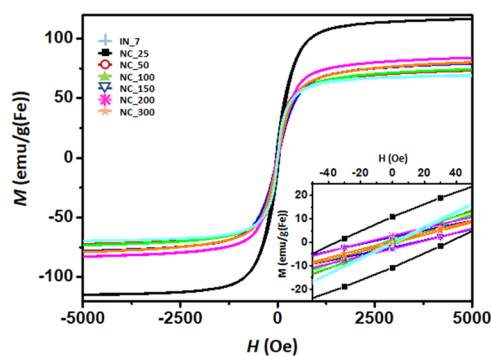


**Figure 4.** *M*-*H* curves of the nanoparticle and NCs measured at 300 K using VSM.

values of all of the nanoparticles and NCs were saturated at an external magnetic field of *ca.*  $\pm 2000$  Oe. The IN\_7 showed superparamagnetic properties with a saturation magnetization of 67 emu·g<sup>-1</sup> (Fe). In contrast, the NCs showed higher saturation magnetizations of 118, 77, 77, 84, 87, and 84 emu·g<sup>-1</sup> (Fe) for NC\_25, NC\_50, NC\_100, NC\_150, NC\_200, and NC\_300, respectively. When the hysteresis graph was magnified from -50 to 50 Oe, NC\_25, NC\_150, and NC\_200

showed ferromagnetic properties, with NC\_25 exhibiting the highest coercivity of 30 Oe. In addition, a shift in blocking temperature in the zero-field cooled (ZFC) curves was observed, and those of NC\_25 and NC\_150 exceeded RT (Figure S8). NC\_50, NC\_100, and NC\_300 exhibited zero coercivity, like IN\_7 (Figure 4, inset). NC\_25 had both the highest coercivity and saturation magnetization among the NCs.

Since the NCs are composed of multiple nanoparticles, investigating the alignment of their crystalline structures would be helpful to understand the magnitude of their magnetization. With this in mind, the crystallographic properties of the NCs were investigated by high-resolution (HR)-TEM (Figure 5).

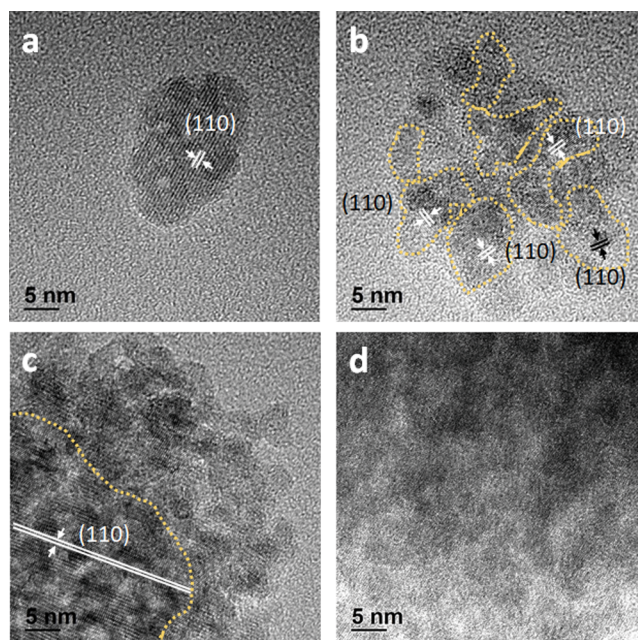


**Figure 5.** HR-TEM images and their corresponding filtered Fourier transforms (FFTs; insets) of (a) NC\_25, (b) NC\_50, (c) NC\_150, and (d) NC\_300. The NCs exhibited well-defined lattice fringes corresponding to the {110} faces.

First, NC\_25 showed a single-crystalline superstructure (Figure 5a), wherein a small number of primary nanoparticles were assembled to form anisotropic NCs (Figure S9). Since the iron oxide nanoparticles clustered on PAA are close to each other, adjacent primary nanoparticles align through an oriented attachment mechanism to reduce their high surface energy.<sup>15,17,29,30,36-41</sup> NC\_50 also showed single-crystalline-like superstructure domains similar to NC\_25, but there were

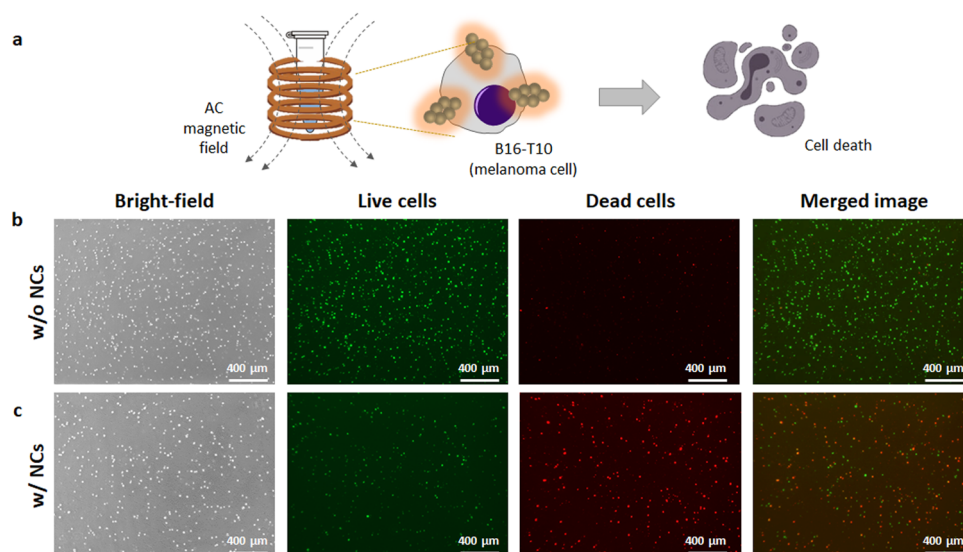


**Figure 6.** (a) Schematic of hyperthermia treatment of melanoma cells (B16-T10) with NC\_25. Bright-field and fluorescence microscopy images of B16-F10 cells under an AC magnetic field and treated (b) without and (c) with NC\_25 stained with calcein and BOBO-3 iodide indicating live cells (green) and dead cells (red), respectively.

some separate lattice domains (yellow dotted lines) where each alignment was slightly tilted (Figure 5b). Increasing the size of the NCs led to inhomogeneous clusters and partially oriented attachment. In the case of NC\_150, each unit particle was a single-crystalline structure, but no oriented attachment was observed at the surface of the NCs. On the other hand, a single-crystalline superstructure was observed in a large part of the core region (Figure 5c). The primary nanoparticles located at the surface of the NCs were more loosely bound than those at the core, and thus, less oriented attachment was observed near the NC surface, as shown in Figure 5c. In the HR-TEM image of NC\_300, the single-crystalline superstructure at its core was difficult to define due to the overlap of many primary nanoparticles (Figure 5d).

The crystalline structures of magnetic particles are an important factor governing their magnetic properties.<sup>40,42,43</sup> NC\_25, which exhibits an oriented attachment in the whole particle, behaves like a single crystal particle due to the effective exchange coupling between magnetic spins in unit nanoparticles,<sup>13,31,44–47</sup> and the anisotropic shape enhances the magnetic anisotropy<sup>47,48</sup> (Figures S10–S12). In addition, the oriented attachment between primary nanoparticles can efficiently reduce the population of surface spins in the NCs. As a consequence, NC\_25 showed ferrimagnetic properties and a superior saturation magnetization,<sup>44,46,49</sup> which might lead to the conversion of heating mechanism from Neel/Brownian relaxation (superparamagnetic materials) to hysteresis loss (ferromagnetic materials). NC\_50 possesses crystallographically aligned domains, which are physically separated and relatively small compared to those of NC\_25. Due to a weak interaction between unit nanoparticles, it also shows superparamagnetic properties and a similar saturation magnetization value to those of IN\_7.<sup>48,50,51</sup> Further, a wide-range single-crystalline superstructure due to oriented attachment at the core region of NC\_150, which possesses ferromagnetic properties, was observed. However, the single-crystalline region is larger than that of the magnetic single domain of iron oxide (*ca.* 20–50 nm),<sup>40,42,52</sup> and thus, a magnetic multidomain would form at the core. In addition, as NC\_150 has surface regions with randomly aligned primary

particles, the spin behavior of NC\_150 at the surface is similar to that of polycrystalline particles. Therefore, the coercivity and saturation magnetization of NC\_150 were smaller than those of NC\_25 even though NC\_150 possessed wider-range crystalline alignment than NC\_25. The magnetic properties that varied in the NCs are important factors that influence various hyperthermia mechanisms such as Neel relaxation and Hysteresis loss.<sup>5</sup> Especially, ferromagnetic materials generate heat through the hysteresis loss, which can be determined with the area of the *M–H* curve. Since the area is proportional to both coercivity and magnetization,<sup>5,53</sup> increasing these two parameters is critical for enhanced hyperthermia effects. Therefore, among the differently sized NCs, NC\_25 exhibited the highest coercivity and saturation magnetization, and thus its hyperthermia effect was highly enhanced compared with those of other NCs (Figure 3b).

Next, we examined the hyperthermia effect of the NCs. Skin cancer cells, B16-F10 ( $1 \times 10^6$  cells), were incubated with NC\_25 under an alternating current (AC) magnetic field for 10 min (Figure 6). In the fluorescence microscopy images, where live and dead cells were stained with Calcein-AM (green) and BOBO-3 iodide (red), respectively, a strong red color was observed with NC\_25 treatment after AC magnetic field application, whereas an intense green color was detected without NC\_25. In addition, our *in vitro* study indicated that no toxic effects occurred with the NCs when an AC magnetic field was not applied, while Co-doped ferrite materials show high cytotoxicity from low concentrations (from 25  $\mu\text{g}\cdot\text{mL}^{-1}$ ) (Figures S13 and S14).

In this study, an effective pure iron oxide-based heat generator for MFH was obtained *via* a facile solvothermal method. When the size of nanoclusters changed, their interparticle crystalline structure was altered, thus influencing the magnetic and hyperthermia properties. Among the prepared NCs, NC\_25, which exhibits the whole range of oriented attachments between primary particles and shape anisotropy, shows the best hyperthermia effect, which was calculated to be three times larger than that of the isolated iron oxide nanoparticles. The verified biocompatibility of NC\_25 may overcome legal hurdles for clinical applications. In



addition, the effective heat generator investigated in this study was produced through a simple and easy synthetic protocol, making mass industrial production possible. Owing to their excellent performance and industrial merits, the designed iron oxide NCs are a fascinating candidate for cancer treatment.

### 3. MATERIALS AND METHODS

**3.1. Materials.**  $\text{FeCl}_3 \cdot 6\text{H}_2\text{O}$ , ethylene glycol, sodium acetate (NaOAc), NaOH, and poly(acrylic acid) (PAA, MW: 5000, 50% aqueous solution) were used as received from Sigma-Aldrich.

**3.2. Synthesis of Nanoclusters (NCs).**  $\text{Fe}_3\text{O}_4$  NCs were synthesized through a solvothermal method. Briefly,  $\text{FeCl}_3 \cdot 6\text{H}_2\text{O}$  (0.68 g) was dissolved in 10 mL of ethylene glycol in the presence of PAA (0.3 g) and NaOAc/NaOH. The mixture was heated to 120 °C for 1 h with vigorous stirring, then transferred to a Teflon-equipped stainless steel autoclave and reacted at 200 °C for 10 h. Molar ratios of NaOAc to NaOH of 1:0.3, 1:0.16, 1:0.1, and 1:0 yielded NC sizes of 25, 50, 100, and 150 nm, which are denoted as NC\_25, NC\_50, NC\_100, and NC\_150, respectively. NC\_200 and NC\_300 were synthesized with reduced amounts of PAA (0.05 and 0.1 g, respectively).

**3.3. Synthesis of 7 nm Iron Oxide Nanoparticles.** The 7 nm iron oxide nanoparticles were synthesized in the solution phase at a high temperature. An NaOH/DEG stock solution was prepared by dissolving NaOH (1 g) in DEG (10 mL), then heated at 120 °C for 1 h under Ar, cooled, and kept at 70 °C. A mixture of PAA (5.184 g),  $\text{FeCl}_3$  (0.065 g), and DEG (17 mL) was heated to 220 °C in a nitrogen atmosphere for 30 min with vigorous stirring. The NaOH/DEG stock solution (1.75 mL) was then injected rapidly into this hot mixture, and the reaction solution slowly turned black. The resulting mixture was further heated for 2 h and then cooled to RT.

**3.4. Characterization.** The morphology and crystallographic alignment of the NCs were observed with a scanning electron microscope (Cold Type FE-SEM, S-4800, Hitachi High Technology, Japan) and a field-emission transmission electron microscope (FE-TEM, Tecnai G<sup>2</sup> F30 S-Twin, FEI, Netherlands). X-ray powder diffraction (XRD) studies were conducted using a Rigaku D/MAX-RB diffractometer equipped with a graphite-monochromatized Cu K $\alpha$  radiation source (40 kV, 120 mA). X-ray photoelectron spectrometry (XPS) was obtained using K $\alpha^+$  XPS (ThermoFisher Scientific). The hydrodynamic size and  $\zeta$ -potential of the NCs were measured using dynamic light scattering (Zetasizer Nano ZS, Malvern). The magnetism of the NCs was measured using a vibrating sample magnetometer (VSM, 7400-S, Lake Shore Cryotronics).

**3.5. Specific Loss Power (SLP) Measurements.** The SLP value of the NCs was measured with a high-radio-frequency heating machine (HF 10K, Taeyang System, Korea), which radiates an alternating magnetic field (AMF) at a frequency ( $f$ ) of 500 kHz and strength of 37.4 kA·m<sup>-1</sup>. An aqueous solution of the NCs (1 mg·mL<sup>-1</sup>) was placed in the center of a water-cooled magnetic induction coil. The time-dependent change in temperature caused by magnetic heating under an AMF was continuously measured with a fiber optic thermometer (M602, LumaSense Technologies). The SLP values (W·g<sup>-1</sup>) of the samples were derived from the equation below

$$\text{SLP} = \frac{CV_s}{m} \frac{dT}{dt}$$

where  $C$  is the volumetric specific heat capacity of the sample solution (J·L<sup>-1</sup>·K<sup>-1</sup>),  $V_s$  is the sample volume (L),  $m$  is the mass of the magnetic material in the sample (g), and  $dT/dt$  is the initial slope of the change in temperature versus time curve (K·s<sup>-1</sup>).

SLP is normalized to intrinsic loss power (ILP) to compare the heating efficiency of magnetic particles measured under external magnetic fields with different experimental amplitudes and frequencies. The ILP values (nH·m<sup>2</sup>·kg<sup>-1</sup>) of the samples were derived from the equation below

$$\text{ILP} = \frac{\text{SLP}}{(f \cdot H^2)}$$

### ■ ASSOCIATED CONTENT

#### Supporting Information

The Supporting Information is available free of charge at <https://pubs.acs.org/doi/10.1021/acsomega.1c04632>.

Summary table of the hyperthermia effects of various materials;  $\zeta$ -potential graphs; XRD patterns; XPS spectrum; aqueous stability examination data; hydrodynamic size of NCs; TEM images and SLP values of IN\_7, IN\_25, and 25 nm nanoassemblies; SEM images and EDS graphs of Co-doped ferrite NCs (Co\_NC); and toxicity tests of NCs and Co\_NC (PDF)

### ■ AUTHOR INFORMATION

#### Corresponding Author

Jin-sil Choi – Department of Chemical and Biological Engineering, Hanbat National University, 34158 Daejeon, Republic of Korea; [orcid.org/0000-0001-9028-8527](https://orcid.org/0000-0001-9028-8527); Email: [jinsil.choi@hanbat.ac.kr](mailto:jinsil.choi@hanbat.ac.kr)

#### Authors

Miseon Jeong – Department of Chemical and Biological Engineering, Hanbat National University, 34158 Daejeon, Republic of Korea

Sanghoon Lee – Department of Chemical and Biological Engineering, Hanbat National University, 34158 Daejeon, Republic of Korea

Dae Young Song – Department of Chemical and Biological Engineering, Hanbat National University, 34158 Daejeon, Republic of Korea

Sunghwi Kang – Center for Nanomedicine, Institute for Basic Science (IBS), 03722 Seoul, Republic of Korea; Department of Chemistry, Yonsei University, 03722 Seoul, Republic of Korea

Tae-Hyun Shin – Research Institute of Radiological Science, Severance Hospital, Yonsei University College of Medicine, 03722 Seoul, Republic of Korea

Complete contact information is available at: <https://pubs.acs.org/doi/10.1021/acsomega.1c04632>

#### Notes

The authors declare no competing financial interest.

### ■ ACKNOWLEDGMENTS

The authors thank Dr. J.-w. Kim for the discussion on the hyperthermia effect of magnetic nanoparticles. This work was

supported by the newly appointed professor research fund of Hanbat National University in 2018 and by National Research Foundation of Korea (NRF) grants funded by the Korean government (MSIT) (2020R1C1C1011863 and 2020R1A5A8017671).

## REFERENCES

- (1) Shah, R. R.; Dombrowsky, A. R.; Paulson, A. L.; Johnson, M. P.; Nikles, D. E.; Brazel, C. S. Determining Iron Oxide Nanoparticle Heating Efficiency and Elucidating Local Nanoparticle Temperature for Application in Agarose Gel-Based Tumor Model. *Mater. Sci. Eng. C* **2016**, *68*, 18–29.
- (2) Deatsch, A. E.; Evans, B. A. Heating Efficiency in Magnetic Nanoparticle Hyperthermia. *J. Magn. Magn. Mater.* **2014**, *354*, 163–172.
- (3) Albarqi, H. A.; Wong, L. H.; Schumann, C.; Sabei, F. Y.; Korzun, T.; Li, X.; Hansen, M. N.; Dhagat, P.; Moses, A. S.; Taratula, O.; Taratula, O. Biocompatible Nanoclusters with High Heating Efficiency for Systemically Delivered Magnetic Hyperthermia. *ACS Nano* **2019**, *13*, 6383–6395.
- (4) Xie, W.; Guo, Z.; Gao, F.; Gao, Q.; Wang, D.; Liaw, B.; Cai, Q.; Sun, X.; Wang, X.; Zhao, L. Shape-, Size- and Structure-Controlled Synthesis and Biocompatibility of Iron Oxide Nanoparticles for Magnetic Theranostics. *Theranostics* **2018**, *8*, 3284–3307.
- (5) Noh, S.; Moon, S. H.; Shin, T.-H.; Lim, Y.; Cheon, J. Recent Advances of Magneto-Thermal Capabilities of Nanoparticles: From Design Principles to Biomedical Applications. *Nano Today* **2017**, *13*, 61–76.
- (6) Hadadian, Y.; Ramos, A. P.; Pavan, T. Z. Role of Zinc Substitution in Magnetic Hyperthermia Properties of Magnetite Nanoparticles: Interplay between Intrinsic Properties and Dipolar Interactions. *Sci. Rep.* **2019**, *9*, No. 18048.
- (7) Jang, J.; Nah, H.; Lee, J.-H.; Moon, S. H.; Kim, M. G.; Cheon, J. Critical Enhancements of MRI Contrast and Hyperthermic Effects by Dopant-Controlled Magnetic Nanoparticles. *Angew. Chem., Int. Ed.* **2009**, *48*, 1234–1238.
- (8) Otero-Lorenzo, R.; Fantechi, E.; Sangregorio, C.; Salgueirino, V. Solvothermally Driven Mn Doping and Clustering of Iron Oxide Nanoparticles for Heat Delivery Applications. *Chem. - Eur. J.* **2016**, *22*, 6666–6675.
- (9) Gupta, R.; Sharma, D. Manganese-Doped Magnetic Nanoclusters for Hyperthermia and Photothermal Glioblastoma Therapy. *ACS Appl. Nano Mater.* **2020**, *3*, 2026–2037.
- (10) Lee, J.-H.; Jang, J.; Choi, J.; Moon, S. H.; Noh, S.; Kim, J.; Kim, J.-G.; Kim, I.-S.; Park, K. I.; Cheon, J. Exchange-Coupled Magnetic Nanoparticles for Efficient Heat Induction. *Nat. Nanotechnol.* **2011**, *6*, 418–422.
- (11) Noh, S.; Na, W.; Jang, J.; Lee, J.-H.; Lee, E. J.; Moon, S. H.; Lim, Y.; Shin, J.-S.; Cheon, J. Nanoscale Magnetism Control via Surface and Exchange Anisotropy for Optimized Ferrimagnetic Hysteresis. *Nano Lett.* **2012**, *12*, 3716–3721.
- (12) Gutiérrez, L.; de la Cueva, L.; Moros, M.; Mazarío, E.; de Bernardo, S.; de la Fuente, J. M.; Morales, M. P.; Salas, G. Aggregation Effects on the Magnetic Properties of Iron Oxide Colloids. *Nanotechnology* **2019**, *30*, No. 112001.
- (13) Kostopoulou, A.; Lappas, A. Colloidal Magnetic Nanocrystal Clusters: Variable Length-Scale Interaction Mechanisms, Synergetic Functionalities and Technological Advantages. *Nanotechnol. Rev.* **2015**, *4*, 595–624.
- (14) Fu, R.; Yan, Y.; Roberts, C.; Liu, Z.; Chen, Y. The Role of Dipole Interactions in Hyperthermia Heating Colloidal Clusters of Densely-Packed Superparamagnetic Nanoparticles. *Sci. Rep.* **2018**, *8*, No. 4704.
- (15) Kostopoulou, A.; Brintakis, K.; Vasilakaki, M.; Trohidou, K. N.; Douvalis, A. P.; Lascialfari, A.; Manna, L.; Lappas, A. Assembly-Mediated Interplay of Dipolar Interactions and Surface Spin Disorder in Colloidal Maghemite Nanoclusters. *Nanoscale* **2014**, *6*, 3764–3776.
- (16) Fuentes-García, J. A.; Diaz-Cano, A. I.; Guillen-Cervantes, A.; Santoyo-Salazar, J. Magnetic Domain Interactions of Fe<sub>3</sub>O<sub>4</sub> Nanoparticles Embedded in a SiO<sub>2</sub> Matrix. *Sci. Rep.* **2018**, *8*, No. 5096.
- (17) Hugounenq, P.; Levy, M.; Alloyeau, D.; Lartigue, L.; Dubois, E.; Cabuil, V.; Ricolleau, C.; Roux, S.; Wilhelm, C.; Gazeau, F.; Bazzi, R. Iron Oxide Monocrystalline Nanoflowers for Highly Efficient Magnetic Hyperthermia. *J. Phys. Chem. C* **2012**, *116*, 15702–15712.
- (18) Pourmiri, S.; Tzitzios, V.; Hadjipanayis, G. C.; Meneses Brassea, B. P.; El-Gendy, A. A. Magnetic Properties and Hyperthermia Behavior of Iron Oxide Nanoparticle Clusters. *AIP Adv.* **2019**, *9*, No. 125033.
- (19) Hayashi, K.; Nakamura, M.; Sakamoto, W.; Yogo, T.; Miki, H.; Ozaki, S.; Abe, M.; Matsumoto, T.; Ishimura, K. Superparamagnetic Nanoparticle Clusters for Cancer Theranostics Combining Magnetic Resonance Imaging and Hyperthermia Treatment. *Theranostics* **2013**, *3*, 366–376.
- (20) Abenojar, E. C.; Wickramasinghe, S.; Bas-Concepcion, J.; Samia, A. C. S. Structural Effects on the Magnetic Hyperthermia Properties of Iron Oxide Nanoparticles. *Prog. Nat. Sci.: Mater. Int.* **2016**, *26*, 440–448.
- (21) Avugadda, S. K.; Materia, M. E.; Nigmatullin, R.; Cabrera, D.; Marotta, R.; Cabada, T. F.; Marcello, E.; Nitti, S.; Artés-Ibañez, E. J.; Basnett, P.; Wilhelm, C.; Teran, F. J.; Roy, I.; Pellegrino, T. Esterase-Cleavable 2D Assemblies of Magnetic Iron Oxide Nanocubes: Exploiting Enzymatic Polymer Disassembling To Improve Magnetic Hyperthermia Heat Losses. *Chem. Mater.* **2019**, *31*, 5450–5463.
- (22) Lattuada, M. Effect of Clustering on the Heat Generated by Superparamagnetic Iron Oxide Nanoparticles. *Chimia Int. J. Chem.* **2019**, *73*, 39–42.
- (23) Ge, J.; Hu, Y.; Biasini, M.; Beyermann, W. P.; Yin, Y. Superparamagnetic Magnetite Colloidal Nanocrystal Clusters. *Angew. Chem., Int. Ed.* **2007**, *46*, 4342–4345.
- (24) Kostopoulou, A.; Tsiaoussis, I.; Lappas, A. Magnetic Iron Oxide Nanoclusters with Tunable Optical Response. *Photonics Nanostruct. - Fundam. Appl.* **2011**, *9*, 201–206.
- (25) Gutiérrez, L.; Costo, R.; Grüttner, C.; Westphal, F.; Gehrke, N.; Heinke, D.; Fornara, A.; Pankhurst, Q. A.; Johansson, C.; Veintemillas-Verdaguer, S.; Morales, M. P. Synthesis Methods to Prepare Single- and Multi-Core Iron Oxide Nanoparticles for Biomedical Applications. *Dalton Trans.* **2015**, *44*, 2943–2952.
- (26) Wetegrove, M.; Witte, K.; Bodnar, W.; Pfahl, D.-E.; Springer, A.; Schell, N.; Westphal, F.; Burkel, E. Formation of Maghemite Nanostructures in Polyol: Tuning the Particle Size via the Precursor Stoichiometry†. *CrystEngComm* **2019**, *21*, 1956–1966.
- (27) Gavilán, H.; Sánchez, E. H.; Brollo, M. E. F.; Asín, L.; Moerner, K. K.; Frandsen, C.; Lázaro, F. J.; Serna, C. J.; Veintemillas-Verdaguer, S.; Morales, M. P.; Gutiérrez, L. Formation Mechanism of Maghemite Nanoflowers Synthesized by a Polyol-Mediated Process. *ACS Omega* **2017**, *2*, 7172–7184.
- (28) Ge, J.; Hu, Y.; Yin, Y. Highly Tunable Superparamagnetic Colloidal Photonic Crystals. *Angew. Chem., Int. Ed.* **2007**, *46*, 7428–7431.
- (29) Cheng, C.; Xu, F.; Gu, H. Facile Synthesis and Morphology Evolution of Magnetic Iron Oxide Nanoparticles in Different Polyol Processes. *New J. Chem.* **2011**, *35*, 1072.
- (30) Lartigue, L.; Hugounenq, P.; Alloyeau, D.; Clarke, S. P.; Lévy, M.; Bacri, J.-C.; Bazzi, R.; Brougham, D. F.; Wilhelm, C.; Gazeau, F. Cooperative Organization in Iron Oxide Multi-Core Nanoparticles Potentiates Their Efficiency as Heating Mediators and MRI Contrast Agents. *ACS Nano* **2012**, *6*, 10935–10949.
- (31) Gavilán, H.; Kowalski, A.; Heinke, D.; Sugunan, A.; Sommertune, J.; Varón, M.; Bogart, L. K.; Posth, O.; Zeng, L.; González-Alonso, D.; Balceris, C.; Fock, J.; Wetterskog, E.; Frandsen, C.; Gehrke, N.; Grüttner, C.; Fornara, A.; Ludwig, F.; Veintemillas-Verdaguer, S.; Johansson, C.; Morales, M. P. Colloidal Flower-Shaped Iron Oxide Nanoparticles: Synthesis Strategies and Coatings. *Part. Part. Syst. Charact.* **2017**, *34*, No. 1700094.
- (32) Sakellari, D.; Brintakis, K.; Kostopoulou, A.; Myrovali, E.; Simeonidis, K.; Lappas, A.; Angelakeris, M. Ferrimagnetic Nanocrystal

Assemblies as Versatile Magnetic Particle Hyperthermia Mediators. *Mater. Sci. Eng. C* **2016**, *58*, 187–193.

(33) Cuenca, J. A.; Bugler, K.; Taylor, S.; Morgan, D.; Williams, P.; Bauer, J.; Porch, A. Study of the Magnetite to Maghemite Transition Using Microwave Permittivity and Permeability Measurements. *J. Phys. Condens. Matter* **2016**, *28*, No. 106002.

(34) Dar, M. I.; Shivashankar, S. A. Single Crystalline Magnetite, Maghemite, and Hematite Nanoparticles with Rich Coercivity. *RSC Adv.* **2014**, *4*, 4105–4113.

(35) Fiévet, F.; Ammar-Merah, S.; Brayner, R.; Chau, F.; Giraud, M.; Mammeri, F.; Peron, J.; Piquemal, J.-Y.; Sicard, L.; Viau, G. The Polyol Process: A Unique Method for Easy Access to Metal Nanoparticles with Tailored Sizes, Shapes and Compositions. *Chem. Soc. Rev.* **2018**, *47*, 5187–5233.

(36) Coral, D. F.; Soto, P. A.; Blank, V.; Veiga, A.; Spinelli, E.; Gonzalez, S.; Saracco, G. P.; Bab, M. A.; Muraca, D.; Setton-Avruij, P. C.; Roig, A.; Roguin, L.; Fernández van Raap, M. B. Nanoclusters of Crystallographically Aligned Nanoparticles for Magnetic Hyperthermia: Aqueous Ferrofluid, Agarose Phantoms and Ex Vivo Melanoma Tumour Assessment. *Nanoscale* **2018**, *10*, 21262–21274.

(37) Cao, S.-W.; Zhu, Y.-J.; Chang, J. Fe<sub>3</sub>O<sub>4</sub> Polyhedral Nanoparticles with a High Magnetization Synthesized in Mixed Solvent Ethylene Glycol–Water System. *New J. Chem.* **2008**, *32*, 1526–1530.

(38) Fang, X.-L.; Chen, C.; Jin, M.-S.; Kuang, Q.; Xie, Z.-X.; Xie, S.-Y.; Huang, R.-B.; Zheng, L.-S. Single-Crystal-like Hematite Colloidal Nanocrystal Clusters: Synthesis and Applications in Gas Sensors, Photocatalysis and Water Treatment. *J. Mater. Chem.* **2009**, *19*, 6154.

(39) Xi, G.; Wang, C.; Wang, X. The Oriented Self-Assembly of Magnetic Fe<sub>3</sub>O<sub>4</sub> Nanoparticles into Monodisperse Microspheres and Their Use as Substrates in the Formation of Fe<sub>3</sub>O<sub>4</sub> Nanorods. *Eur. J. Inorg. Chem.* **2008**, *2008*, 425–431.

(40) Reichel, V.; Kovács, A.; Kumari, M.; Bereczk-Tompa, É.; Schneck, E.; Diehle, P.; Pósfai, M.; Hirt, A. M.; Duchamp, M.; Dunin-Borkowski, R. E.; Faivre, D. Single Crystalline Superstructured Stable Single Domain Magnetite Nanoparticles. *Sci. Rep.* **2017**, *7*, No. 45484.

(41) Javed, Y.; Lartigue, L.; Hugounenq, P.; Vuong, Q. L.; Gosuain, Y.; Bazzi, R.; Wilhelm, C.; Ricolleau, C.; Gazeau, F.; Alloyeau, D. Biodegradation Mechanisms of Iron Oxide Monocrystalline Nanoflowers and Tunable Shield Effect of Gold Coating. *Small* **2014**, *10*, 3325–3337.

(42) Li, Q.; Kartikowati, C. W.; Horie, S.; Ogi, T.; Iwaki, T.; Okuyama, K. Correlation between Particle Size/Domain Structure and Magnetic Properties of Highly Crystalline Fe<sub>3</sub>O<sub>4</sub> Nanoparticles. *Sci. Rep.* **2017**, *7*, No. 9894.

(43) Prabhakaran, D.; Boothroyd, A. T.; Coldea, R.; Helme, L. M. Magnetic Studies of Polycrystalline and Single-Crystal Na<sub>x</sub>Co<sub>2</sub>. *J. Appl. Phys.* **2011**, *109*, No. 07E146.

(44) Suzuki, M.; Fullem, S. I.; Suzuki, I. S.; Wang, L.; Zhong, C.-J. Observation of Superspin-Glass Behavior in Fe<sub>3</sub>O<sub>4</sub> Nanoparticles. *Phys. Rev. B* **2009**, *79*, No. 024418.

(45) Parker, D.; Dupuis, V.; Ladiou, F.; Bouchaud, J.-P.; Dubois, E.; Perzynski, R.; Vincent, E. Spin-Glass Behavior in an Interacting  $\gamma$ -Fe<sub>2</sub>O<sub>3</sub> Nanoparticle System. *Phys. Rev. B* **2008**, *77*, No. 104428.

(46) Bender, P.; Honecker, D.; Fernández Barquín, L. Supraferromagnetic Correlations in Clusters of Magnetic Nanoflowers. *Appl. Phys. Lett.* **2019**, *115*, No. 132406.

(47) Bender, P.; Fock, J.; Frandsen, C.; Hansen, M. F.; Balceris, C.; Ludwig, F.; Posth, O.; Wetterskog, E.; Bogart, L. K.; Southern, P.; Szczerba, W.; Zeng, L.; Witte, K.; Grüttnert, C.; Westphal, F.; Honecker, D.; González-Alonso, D.; Fernández Barquín, L.; Johansson, C. Relating Magnetic Properties and High Hyperthermia Performance of Iron Oxide Nanoflowers. *J. Phys. Chem. C* **2018**, *122*, 3068–3077.

(48) Niculaes, D.; Lak, A.; Anyfantis, G. C.; Marras, S.; Laslett, O.; Avugadda, S. K.; Cassani, M.; Serantes, D.; Hovorka, O.; Chantrell, R.; Pellegrino, T. Asymmetric Assembling of Iron Oxide Nanocubes for Improving Magnetic Hyperthermia Performance. *ACS Nano* **2017**, *11*, 12121–12133.

(49) Hiroi, K.; Kura, H.; Ogawa, T.; Takahashi, M.; Sato, T. Spin-Glasslike Behavior of Magnetic Ordered State Originating from Strong Interparticle Magnetostatic Interaction in  $\alpha$ -Fe Nanoparticle Agglomerate. *Appl. Phys. Lett.* **2011**, *98*, No. 252505.

(50) Bender, P.; Wetterskog, E.; Honecker, D.; Fock, J.; Frandsen, C.; Moerland, C.; Bogart, L. K.; Posth, O.; Szczerba, W.; Gavilán, H.; Costo, R.; Fernández-Díaz, M. T.; González-Alonso, D.; Fernández Barquín, L.; Johansson, C. Dipolar-Coupled Moment Correlations in Clusters of Magnetic Nanoparticles. *Phys. Rev. B* **2018**, *98*, No. 224420.

(51) Serantes, D.; Simeonidis, K.; Angelakeris, M.; Chubykalo-Fesenko, O.; Marciello, M.; Morales, M. d. P.; Baldomir, D.; Martínez-Boubeta, C. Multiplying Magnetic Hyperthermia Response by Nanoparticle Assembling. *J. Phys. Chem. C* **2014**, *118*, 5927–5934.

(52) Castellanos-Rubio, I.; Rodrigo, I.; Munshi, R.; Arriortua, O.; Garitaonandia, J. S.; Martínez-Amesti, A.; Plazaola, F.; Orue, I.; Pralle, A.; Insausti, M. Outstanding Heat Loss via Nano-Octahedra above 20 nm in Size: From Wustite-Rich Nanoparticles to Magnetite Single-Crystals. *Nanoscale* **2019**, *11*, 16635–16649.

(53) Jeun, M.; Lee, S.; Kim, Y. J.; Jo, H. Y.; Park, K. H.; Paek, S. H.; Takemura, Y.; Bae, S. Physical Parameters to Enhance AC Magnetically Induced Heating Power of Ferrite Nanoparticles for Hyperthermia in Nanomedicine. *IEEE Trans. Nanotechnol.* **2013**, *12*, 314–322.